Macromolecules

ARTICLE

pubs.acs.org/Macromolecules

Cyclic or Permanent? Structure Control of the Contraction Behavior of Regenerated *Bombyx mori* Silk Nanofibers

Taiyo Yoshioka,[†,§] Yutaka Kawahara,[‡] and Andreas K. Schaper*[,†]

[†]Materials Science Center, EM&Mlab, Philipps University of Marburg, Hans-Meerwein-Str., 35032 Marburg, Germany

[‡]Department of Biological and Chemical Engineering, Gunma University, 1-5-1 Tenjin-cho, Kiryu, Gunma 376-8515, Japan

Supporting Information

ABSTRACT: The interest in the physics and chemistry of natural silk is due to the extraordinary mechanical, chemical, and biological properties and high functionality of this material. In particular, its unique mechanical behavior, which has never been realized in man-made fibers so far, makes the silk so attractive for materials scientists. We report here the occurrence of pure cyclic contraction in fibroin nanofibers electrospun from regenerated *Bombyx mori* silk. Evidence is presented of the essential role the oriented noncrystalline molecular chains and the water-soluble silk-I crystal modification play in this reversible mechanical process. We also show that regenerated silk may permanently supercontract if it contains a minimum amount of silk-II β-crystals.

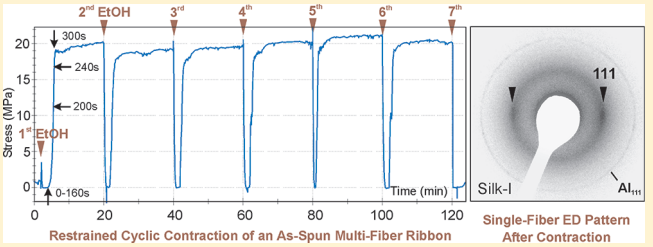

INTRODUCTION

Spider dragline silk shows significant shrink of ~50% and more of its original length, a decrease in Young's modulus and yield strength, and an increase of the strain to fracture when the fiber is wetted in the unrestrained state.[1−5] This behavior is known as "supercontraction" and is generally interpreted as the result of water-induced breaking of interchain hydrogen bonds and subsequent entropy-driven recoiling of oriented amorphous chains.[6−10] Apart from changes in orientation, the β-crystalline regions are supposed not to contribute essentially to the contraction behavior because of the crystal interiors being widely impermeable to humidity.[6−8,11] Vice versa, supercontraction generates substantial stress up to 50 MPa if the fibers are under restrained conditions.[12−14] In the former case, supercontraction was found to be recoverable by stretching of the fibers when they are still in the wet state and then drying. The structure of restrained fibers, on the other hand, has been shown to undergo irreversible changes at relative humidity exceeding ~70%; the original state cannot be restored in this case.[14−16]

The property of supercontraction has long been associated exclusively with major ampullate *Nephila clavipes* spider dragline silk.[17] Recently, Plaza et al.[18] first published significant supercontraction of 13% also in fibers spun from regenerated *Bombyx mori* silkworm silk, in contrast to <3% of the natural counterpart fibers and even of 24% when a special postwet-stretching treatment was applied.[19] While the fundamentals of supercontraction have not yet been completely clarified until now, the situation has become even more complex due to the recent observations by Blackledge et al.[15,16] of the phenomenon of reversible contraction in response to cyclic wetting and drying of spider dragline silk.

In the present contribution, we have applied the electrospinning method to fabricate micro- and nanofibers from regenerated *Bombyx mori* silk fibroin and have performed systematic studies of the influence of the supermolecular structure on the contraction behavior under alcohol or water vapor conditions. Particular focus is cast on the cyclic reaction to changes in hymidity of the regenerated silk fibers and on the appearance of supercontraction under restrained conditions. On the basis of the results of mechanical measurements with nanofiber ribbons of contraction stress and tensile properties, and of structural examinations using wide-angle X-ray diffraction (WAXD) of fiber bundles and transmission electron diffraction (TED) of single nanofibers, we develop a model of the contraction mechanisms in regenerated silk fibers.

EXPERIMENTAL SECTION

Materials. *Bombyx mori* silk fibers were degummed in high pressurized water at 120 °C for 1 h. The degummed fibroin fiber material was dissolved in the ternary solvent system $CaCl_2/CH_3CH_2OH/H_2O$ (mole ratio 1:2:8) at a temperature of 75 °C for 15 min. Afterward, the solution was dialyzed for 4 days using a cellulose tube at 25 °C, filtrated, and lyophilized. The resultant fibroin sponge was then dissolved in 1,1,1,3,3,3-hexafluoro-2-propanol (HFIP), a 5 wt % solution was prepared for electrospinning. All reagents used here were purchased from Sigma-Aldrich. The cellulose dialysis tube, cutoff at molecular weight 14 000, was purchased from Viskase Sales Corp.

Electrospinning of Nanofibers. The fibroin solution was electrospun at a spinning distance of 100 mm and an applied voltage of 10 kV. The nanofibers in the diameter range 180−260 nm were collected in a parallel fashion using a rotating disk collector of 200 mm diameter at a take-up speed of 10 m/s. The collected fiber mat of 10 mm width was carefully detached from the collector and was cut into 40 mm long ribbons.

Received: June 22, 2011
Revised: August 9, 2011
Published: August 26, 2011

Measurements of Contraction Stress and Tensile Properties. The measurements of contraction stress and tensile properties were performed in a tensile testing machine (Zwick Roell, Germany) with the ribbon fastened through clamps by 10 mm at both ends avoiding any significant slack or stress. The remaining test length of 20 mm was kept constant during the measurements of contraction stress. Wetting was carried out gently from one side of the ribbon using ca. 0.1 mL of ethanol (EtOH) and a versatile syringe. The one-sided treatment was sufficient for complete wetting of the whole ribbon at once. The restrained contraction changes the ribbon shape from rectangular into dumbbell-like form, 25 × 4 mm^2 test specimens were cut out of the central part of the dumbbells for the tensile tests. In all tensile tests a cross-head speed of 2 mm/min was applied; the results are average values obtained from five specimens in each case. The true stress was calculated from the ribbon weight, its geometrical dimensions, and the fibroin density (1.25 g/cm^3).[20] Actually, we have to consider changes in density occurring during the contraction process; the effect on the resultant stress is, however, expected to be less than 10% which is why it was ignored here. All measurements were carried out under laboratory room conditions of 40% relative humidity and a temperature of 23 °C.

Structure Studies. WAXD measurements were performed using a D5000/Diffracplus diffractometer (Siemens, Germany) and Cu Kα radiation recording a 2θ diffraction range of 5°−35°. For ED analysis single as-spun nanofibers were collected between two parallel metal plates fixed on the circumference of the rotation collector disk at a 10 mm gap distance (two-bladed "water wheel"). The rotation take-up speed was 10 m/s; the collection was restricted to only one layer of independent parallel-aligned nanofibers. Part of the fibers were crystallized by exposing to water vapor (WV) for 2 h at 70 °C in the unrestrained state. In order to stabilize specimens against the electron beam, copper grids with carbon support film were used. Calibration of the diffraction patterns was done using thin aluminum coating as a standard. The ED studies were performed in a transmission electron microscope JEM-3010 (JEOL Ltd., Japan) at an accelerating voltage of 300 kV using a slow scan CCD camera (Gatan Inc.) for image recording.

■ RESULTS AND DISCUSSION

Figure 1a shows the typical cyclic stress response of a nanofiber ribbon to alternating wetting with EtOH and subsequent air drying in the restrained state, i.e., while the ribbon being fixed at both ends. A highly regular cyclic stress course over time was detected; the arrows indicate the stages of EtOH soaking. The six treatment cycles shown could be continued with negligible changes through many repeats. Every EtOH soaking causes complete relaxation of the nanofiber ribbon; every fast drying tenses the ribbon and produces an average drawing or contraction stress of about 20 MPa, which corresponds to ∼60% of the yield strength of the original ribbon. In each case the tensional force is retained at almost constant level after the drying process has been completed. The cyclic response is considered purely reversible; no indications of supercontraction were observed at all. To make the definitions clear, the term "supercontraction" has been used to describe the contraction occurring during wetting in general,[1−5] but it has recently been applied by Blackledge et al.[15,16] to denote a contraction process that is accompanied by permanent structural changes, in contrast to the reversible changes which occur in the drying stage during "cyclic contraction".

During progressive cycling the ribbon macroscopically changes in shape as shown by the time-resolved photographic image series in Figure 1b corresponding to the subsequent treatment stages marked in Figure 1a. These changes are expression of a rising tensile stress in response to the constraint imposed onto the fibers

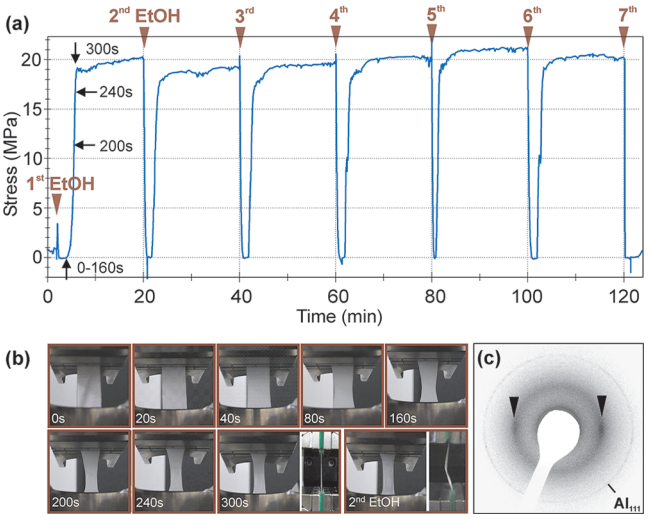

Figure 1. (a) Typical contraction stress vs time characteristics showing pure cyclic contraction of a restrained ribbon of parallel-aligned regenerated fibroin nanofibers. The subsequent stages of EtOH soaking 1−7 are marked by arrow heads. (b) Photographic images of the sequence changes in ribbon shape during the 300 s of the first contraction cycle and of the start of second EtOH wetting along with the side views of the relaxed ribbon before and after this wetting stage. (c) Single-fiber electron diffraction pattern of an individual regenerated fibroin fiber EtOH-treated in the restrained state showing the equatorial 111 reflection arcs of the oriented crystalline silk-I phase.

within the ribbon against contraction. In the first cycle the shape of the ribbon changed from rectangular to dumbbell-like during drying, but upon subsequent EtOH soaking and relaxation it did not entirely revert to the original rectangular shape because of physical adhesion between neighboring nanofibers. Side views of the ribbon in Figure 1b before and after the second wetting are proof of complete relaxation. The very similar behavior of nanofiber bundles (see Supporting Information, Figure SI.1), prepared by rolling up of the ribbon in the direction perpendicular to the fiber axis, demonstrates that the basic contraction process is an intrinsic property of each single nanofiber and must not be addressed to the macroscopic shape deformation of the ribbon. The equatorial intensity arcs in electron diffraction of an EtOH-treated single fiber in Figure 1c reveal crystal-like chain orientation within the deformed fibers (see below, compare ref 21). While the same experiments, except using water instead of EtOH soaking, lead to immediate dissolution and breaking of the ribbon due to the much larger dipole moment of water and hence stronger interaction with the hydrogen bonds, a WV treatment causes contraction quite similar to EtOH as to changes in stress, shape, and structure. However, because a system to accurately control the WV treatment has not yet been established, only the results obtained using EtOH soaking are reported here.

The tensile properties of numerous as-spun nanofiber ribbons were determined before (a) and after (b) restrained EtOH treatment and are presented in Figure 2. The tensile stress of a ribbon directly relates to the contraction of the regenerated fibroin nanofibers. Each single contraction following wetting by EtOH yielded a drastic increase in average Young's modulus from 1.4 to 3.2 GPa, and in yield strength from 33.6 to 96.1 MPa; the fracture strain in parallel decreased from about 8.7% to 3.7%. To our knowledge, the upper modulus and strength values are among the highest observed in electrospun nanofiber mats of

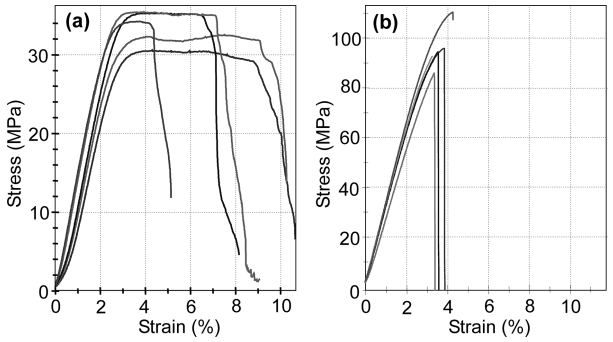

Figure 2. Stress−strain curves of numbers of as-spun regenerated-fibroin nanofiber ribbons (a) before and (b) after one cycle of restrained contraction induced by EtOH soaking and drying.

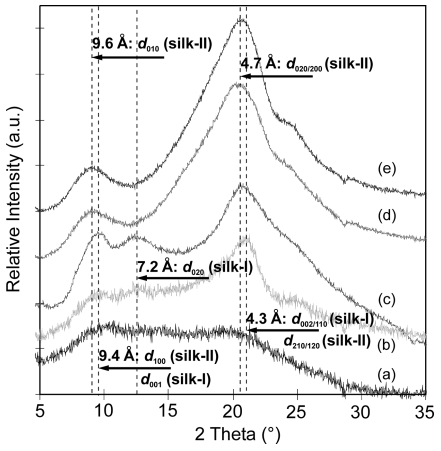

Figure 3. WAXD curves of the as-spun amorphous regenerated-fibroin multifiber ribbon (a), of a ribbon which was WV-treated (b) or EtOH-treated (c) at 70 °C for 2 h in the restrained state, and of ribbons which were treated using EtOH (d) or WV (e) at 70 °C for 2 h in the unrestrained state. The relevant diffraction features are annotated.

regenerated silk fibroin yet[20] but are still considerably lower than the values of force drawn and pristine natural silkworm fibers.[22] The measurements suggest that the improved mechanical properties are caused by an increase in orientation and packing density of amorphous chains in the course of restrained contraction. At this place, an excursion into nature's workshop is most instructive. *Bombyx mori* produces the silk fiber by means of repeatedly attaching the spinning dope on the inside cocoon surface and stretching the freshly formed thread through a figure of eight motion of its head.[23] During solvent evaporation the stretched thread undergoes restrained contraction like the orientation-collected electrospun fibers in the present artificial process, however, influenced by the composite skin-core structure of the native fiber. Since the adhesion to the cocoon surface is transferred via the outer sericin fiber skin, the restrictions on chain movement during contraction are partly neutralized in the fibroin core. This should promote silk-II crystallization (see below) and, hence, result in a noticeably higher strength level (∼500 MPa[22]) than in the case of our regenerated fibroin fibers with temporary silk-I structure (∼100 MPa).

Figure 3 provides wide-angle X-ray diffraction (WAXD) information about the structural changes that have occurred within a restrained fiber due to contraction by WV (curve *b*) and EtOH (curve *c*), in comparison to the widely amorphous as-spun fiber (curve *a*). The EtOH treatment under restrained condition of the original fibers has induced a weak crystalline structure with significant maxima around 2θ ∼9.5° (d = 9.4 Å), 2θ ∼12.3° (d = 7.2 Å), and 2θ ∼ 21.2° (d = 4.3 Å) not present in the as-spun fiber. Among these reflections, the peak at 2θ ∼ 12.3° agrees well with the 020 lattice plane scattering of the orthorhombic (monoclinic) silk-I crystal structure with the lattice parameters a = 4.65 Å, b = 14.24 Å, c = 8.88 Å, and $\gamma \approx 90°$ as determined by Okuyama et al.[24] and Asakura et al.[25,26] (see also refs 27 and 28). There is no peak overlapping by silk-II scattering (curves *d* and *e*, see below) that could be misleading within this angular region.[29] Of the other silk-I-related two peaks in Figure 3, the first one near 9.5° may be due to the 001 reflection of silk-I and/or the 100 reflection of silk-II and the second peak around 21° the 002/110 reflections of silk-I and several *hk*0 reflections of silk-II. The 001 reflection of silk-I should theoretically be forbidden due to structure factor extinction of the space group $P2_12_12_1$[24] but may nevertheless practically occur if the crystals accommodate strain or they contain imperfections. By these reasons, clear assignment of the peaks of curves *b* and *c* proves straightforward merely for the one at 2θ ∼12.3° serving as an unambiguous sign of the presence of the silk-I phase. Additional proof of the silk-I phase is provided by the electron diffraction of an EtOH-treated single fiber in Figure 1c, showing equatorial reflection arcs at 3.95 Å spacing which exactly fits the 111 lattice plane scattering (d = 3.95 Å) of the silk-I structure. The α-helical structure with reflections located at 4.7 and 5.6 Å found in films cast from HFIP solution by Drummy et al.[30] has not been observed here.

Silk-I has been described as an intermediate crystal phase occurring in the early liquid-like state of the fibroin spinning solution within the silkworm glands, which transforms into the crystalline β-structure in the course of fiber formation.[31] Since silk-I crystals are known to be metastable and water-soluble,[32,33] their repeated formation out of the oriented chains in the amorphous regions under constraint is considered quite a reasonable conformational transition facilitating cyclic contraction. That this transition may occur without any irreversible contributions agrees with the assumption of Liu et al.[6] according to which also eventually formed silk-II crystallites and poorly defined crystalline fragments become disintegrated by EtOH soaking and will, thus, not obstruct the pure cyclic process.

The regenerated silk fibers exhibit a totally different behavior when their structure is crystalline instead of near-amorphous or, more precisely, partially crystalline containing a considerable amount of silk-II modification. Transformation into a β-crystal-rich state was achieved according to Magoshi et al.[34] by treating the as-spun fibers with WV at a temperature of 70 °C for 2 h under unrestrained conditions. Electron diffraction in Figure 4a,b of an individual nanofiber verifies a β-crystalline texture comprising the typical reflections of the monoclinic lattice of space group $P2_1$. Strong intensity peaks are the equatorial 020/200 and 210/120 reflections with their higher off-meridional orders 211/121 and 213/123 and the 006 meridional arcs of the 6-fold repeat of the peptide chain residues. The pattern is well described by the unit cell parameters a = 9.38 Å, b = 9.49 Å, c = 6.98 Å, and $\gamma \approx 90°$ after Takahashi et al.[35] and Martel et al.[36] The ED results are confirmed by the WAXD analysis of a nanofiber ribbon in Figure 3 (curve *e*). Curve *d* of the diagram also demonstrates that EtOH instead of WV has a very similar but less pronounced effect onto the unrestrained fiber structure. The response to alternating EtOH wetting and drying of this highly crystalline structure is

represented in Figure 4c. The measuring stress vs time curve reveals contraction during the wetting phase, and partial relaxation during drying of a restrained ribbon composed of silk-II-rich fibers, as opposed to the inverse behavior of initially noncrystalline samples as in Figure 1 and also of fiber ribbons pretreated in the restrained state with WV as in Figure 3b (see Supporting Information, Figure SI.2). The dominating irreversible component, indicated by up/down arrows in Figure 4c, is largest in the first contraction cycle but becomes reduced stepwise during following cycles of EtOH soaking until it seems approaching a constant level after the fifth cycle. Accumulation of the irreversible contraction events results in a total stress of ~2.8 MPa. This type of contraction bears all signs of true "supercontraction" characterized by an irreversible uptake of alcohol (or water) which permanently binds to the fibroin chains. In their recent paper, Blackledge et al.[15] observed spider dragline silk permanently increased in mass by ~1%, against ~1.6 ± 0.5% of total mass increase, which means that part of the mass gained during supercontraction was lost when humidity decreased again. In Figure 4c, we show that in our regenerated silk an almost constant portion of ~0.5 MPa out of the total 2.8 MPa contraction relaxes during drying. This reversible portion is considered the only contraction effect remaining when the capability of the fibers further to supercontract has become used up after a few cycles.

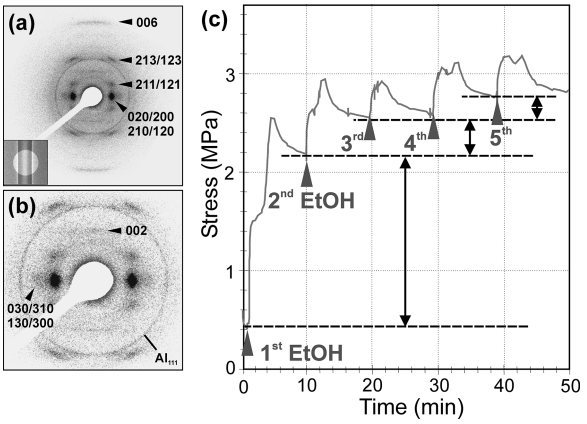

Figure 4. Oriented electron diffraction pattern obtained from a single nanofiber crystallized in the β-sheet crystal formation by applying a WV-treatment at 70 °C for 2 h in the unrestrained state: (b) is an enlargement of (a). Stress vs time diagram (c) of a restrained ribbon composed of crystalline nanofibers such as documented in (a) showing characteristic supercontraction behavior in a repeated EtOH wetting treatment and partial relaxation during the drying phase. The up/down arrows indicate the irreversible supercontraction events, and the upward arrows mark the stages of EtOH soaking.

The observations of the contractional behavior of regenerated *Bombyx mori* silk are summarized in Figure 5. It is widely accepted that both spider and silkworm silk fibers show a distinctive hierarchical structure composed of bundles of micro- and nanofibrils[37−41] built up by a network of oriented chains which interconnect rigid regions of β-sheet crystallites, transferred by flexible molecular spacer regions. As is known from the fabrication of man-made fibers, e.g., polyethylene,[42] electrospinning favors the formation of nanofibrillar morphologies with basic network structure. However, contrary to the crystallization emerging during solution spinning of polyethylene, the formation of extended long-range ordering and of β-sheet crystalline regions is usually suppressed in the spinning of regenerated silk fibroin. Here, amorphous chains dominate the final network structure in coiled matrix conformations (thin margenta line in Figure 5) or in a partially extended conformation with orientation parallel to the fiber axis (thick green line in Figure 5), along with small β-crystal nuclei and interchain hydrogen bonds as linker points.[37,43,44] The chain orientation is the result of tensile deformation during rotating disk collection of the as-spun fiber at a take-up speed of 10 m/s[45] which is manifested in the observed decrease of the average fiber diameter by ~40%. Further evidence of a certain amount of well-aligned chains in the as-spun nanofibers is provided by the high orientation ED pattern in Figure 4, obtained from a WV-treated fiber under unrestrained conditions. Obviously, the main network structure and its orientation are maintained even after exposure to WV.

The cyclic restrained contraction is assumed to originate from the strong affinity of EtOH to the hydrophilic amino acids in the amorphous chain regions,[15] where it disrupts interchain hydrogen bonds during wetting with EtOH (Figure 5a,b). By this rupture,

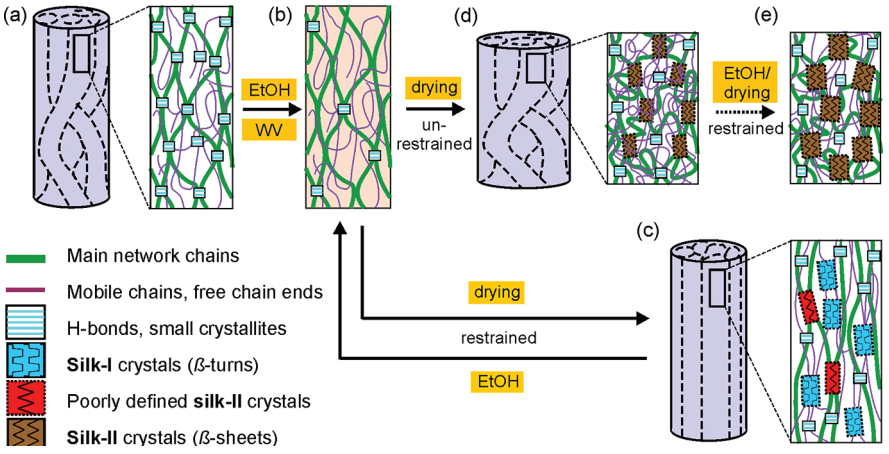

Figure 5. Proposed molecular model of the contraction of as-spun regenerated fibroin nanofibers (a), induced by EtOH or WV wetting (b) and subsequent drying under either restrained (c) or unrestrained (d) conditions. The cyclic response to alternating humidity conditions in the restrained state is determined by the formation of silk-I and poorly defined silk-II crystals out of the amorphous chain content, and their subsequent disintegration during wetting (b, c). The latter process was proved highly repeatable. Unrestrained drying leads to the development of silk-II β-crystallinity (d), which can become stepwise enhanced by lamellar overgrowth during supercontraction initiated by repeated EtOH wetting and drying of the restrained fibers (e).

dx.doi.org/10.1021/ma2014172 |*Macromolecules* 2011, 44, 7713–7718

constraints in the network are released. The subsequent drying process allows the re-formation of H-bonding and the generation of new constraints in the amorphous regions leading to an increase in the measured stress. However, these features on their own cannot explain the pronounced cyclic behavior of our noncrystalline low-strength fibroin fibers. The experimental findings rather suggest that the cyclic phenomenon is closely related to the occurrence of the silk-I crystal phase after EtOH uptake (Figure 5c). Since the β-turn configuration of the silk-I chains implicates intramolecular as well as intermolecular hydrogen bonding,[26] repeated disintegration of the silk-I crystals during wetting and their recrystallization during drying may occur very likely. Therefore, the silk-I cycle is proposed to be the key mechanism in the reversible contraction of regenerated silk; destruction and re-formation of intermolecular hydrogen bonds between single amorphous chains may additionally play a role. In this connection, the reversible crystallization and disintegration are considered to occur mainly within regions just above and below the linking points of the principal network structure where the amorphous chains are thought to be more highly aligned and densely packed than in regions far from the linkers.[43] For the sake of simplicity, this is, however, not reflected in part (c) of the model image Figure 5. The crystallization of silk-I and the improved alignment of amorphous chains both energetically stabilize the composite silk structure and result in its superb stiffness and strength values given in Figure 2.

A certain degree of pleated-sheet β-crystallinity as was introduced here by 2 h WV treatment at 70 °C of the unrestrained initial fibers (compare Figure 5d) is considered a necessary prerequisite for supercontraction to occur. The silk-II crystals are generally not affected by humidity, and the constraints they exert on the chains in the amorphous matrix regions reduce the ability of these chains to undergo entropic contraction. The limited chain mobility could explain the rather small rise in stress upon supercontraction. However, we suggest that the presence of the silk-II crystals has another important effect. It is energetically favorable for the free amorphous chains which have become partially mobilized during wetting to form crystal overgrowths. As illustrated in Figure 5e, the total silk-II crystallinity as well as the crystal sizes gradually increases with progressing overgrowth, which *per se* causes a stepwise reduction in the capability to supercontraction and thus confines the overall permanent contraction to a constant level after a limited number of wetting cycles. In this context it is interesting to note that natural *Bombyx mori* silk, which has much higher silk-II crystallinity than the present regenerated fibroin nanofibers, and even than spider dragline silk,[46] does not show any perceptible supercontraction. The partial relaxation recorded in Figure 4c of the restrained contraction stress during successive drying steps finds its explanation in a certain restoration of local chain orientations and in a likely creep deformation of the crystal overgrowths.

CONCLUSIONS

In conclusion, our experimental observations suggest that pure cyclic contraction of regenerated fibroin requires an initially noncrystalline structure of highly oriented chains. A structure like this is produced in electrospinning which includes the spinning process from solution and a collection-induced structure alignment. We postulate that the unusual cyclic behavior of the electrospun fibroin nanofibers is governed by the formation dynamics of the silk-I modification and by the mobility of the amorphous chains. We have also obtained clear indications that enhanced β-crystallinity is an essential prerequisite for the supercontractional effect to operate. Beside silk's biocompatibility, the mechanical properties of silk-based materials, particularly the amazing cyclic behavior, show promise of successful exploitation in biomimetic and other applications, such as artificial muscles or tendons, scaffolds for tissue engineering and wound healing, sutures for neurosurgery, or nanoscopic sensor devices.[16,47] Feasibility of such developments is provided by the available large quantities of natural silkworm raw material for the fabrication of regenerated silk fibers and by the technique of electrospinning, which admits tailoring of the fiber products. Future challenges of research in this field will include the synthesis of appropriate protein spinning dopes for the fabrication of completely artificial silk fibers.[17,47,48]

ASSOCIATED CONTENT

Supporting Information. Plot of stress vs time characteristics of the EtOH wetting/drying behavior of a restrained nanofiber bundle (Figure SI.1); plot of stress vs time characteristics of the cyclic EtOH wetting/drying behavior of a nanofiber ribbon pre-treated in WV under restrained condition (Figure SI.2). This material is available free of charge via the Internet at http://pubs.acs.org.

AUTHOR INFORMATION

Corresponding Author

*E-mail: schaper@staff.uni-marburg.de.

Present Addresses

[§]Graduate School of Engineering, Toyota Technological Institute, 2-12-1 Hisakata, Tempaku, Nagoya 468-8511, Japan.

ACKNOWLEDGMENT

A.K.S. thanks Prof. M. Tsuji (Institute for Chemical Research, Kyoto University) for stimulating this research work and for long-standing generous cooperation. T.Y. gratefully acknowledges a fellowship from the Alexander von Humboldt Foundation (Germany) which made the present project possible. The authors are indebted to Dr. R. Dersch (Department of Chemistry, Philipps University of Marburg) for his expert assistance during electrospinning experiments and to Mrs. J. Moll (Max Planck Institute of Terrestrial Microbiology, Marburg) for her help in preparation of the regenerated fibroin.

REFERENCES

(1) Work, R. W. *Text. J. Res.* **1977**, *47*, 650–662.
(2) Work, R. W. *J. Arachnol.* **1981**, *9*, 299–308.
(3) Pérez-Rigueiro, J.; Elices, M.; Guinea, C. V. *Polymer* **2003**, *44*, 3733–3763.
(4) Elices, M.; Pérez-Rigueiro, J.; Plaza, G.; Guinea, G. V. *J. Appl. Polym. Sci.* **2004**, *92*, 3537–3541.
(5) Guinea, G. V.; Elices, M.; Pérez-Rigueiro, J.; Plaza, G. R. *J. Exp. Biol.* **2005**, *208*, 25–30.
(6) Liu, Y.; Shao, Z.; Vollrath, F. *Nature Mater.* **2005**, *4*, 901–905.
(7) Shao, Z.; Vollrath, F.; Sirichaisit, J.; Young, R. J. *Polymer* **1999**, *40*, 2493–2500.
(8) Simmons, H.; Michal, C. A.; Jelinski, L. W. *Science* **1996**, *271*, 84–87.
(9) Grubb, D. T.; Ji, G. *Int. J. Biol. Macromol.* **1999**, *24*, 203–210.
(10) Eles, P. T.; Michal, C. A. *Macromolecules* **2004**, *37*, 1342–1345.

(11) Work, R. W.; Morosoff, N. *Text. Res. J.* **1982**, *52*, 349–356.
(12) Bell, F. I.; McEwen, I. J.; Viney, C. *Nature* **2002**, *416*, 37.
(13) Savage, K. N.; Guerette, P. A.; Gosline, J. M. *Biomacromolecules* **2004**, *5*, 675–679.
(14) Agnarsson, I.; Boutry, C.; Wong, S. C.; Baji, S.; Dhinojwala, A.; Sensenig, A. T.; Blackledge, T. A. *Zoology* **2009**, *112*, 325–331.
(15) Blackledge, T. A.; Boutry, C.; Wong, S. C.; Baji, A.; Dhinojwala, A.; Sahni, V.; Agnarsson, I. *J. Exp. Biol.* **2009**, *212*, 1981–1989.
(16) Agnarsson, I.; Dhinojwala, A.; Sahni, V.; Blackledge, T. A. *J. Exp. Biol.* **2009**, *212*, 1990–1994.
(17) Fu, C.; Shao, Z.; Vollrath, F. *Chem. Commun.* **2009**, 6515–6529.
(18) Plaza, G. R.; Corsini, P.; Pérez-Rigueiro, J.; Marsano, E.; Guinea, G. V.; Elices, M. *J. Appl. Polym. Sci.* **2008**, *109*, 1793–1801.
(19) Plaza, G. R.; Corsini, P.; Marsano, E.; Pérez-Rigueiro, J.; Biancotto, L.; Elices, M.; Riekel, C.; Agulló-Rueda, F.; Gallardo, E.; Calleja, J. M.; Guinea, G. V. *Macromolecules* **2009**, *42*, 8977–8982.
(20) Gandhi, M.; Yang, H.; Shor, L.; Ko, F. *Polymer* **2009**, *50*, 1918–1924.
(21) Kawahara, Y.; Nakayama, A.; Matsumura, N.; Yoshioka, T.; Tsuji, M. *J. Appl. Polym. Sci.* **2008**, *107*, 3681–3684.
(22) Shao, Z.; Vollrath, F. *Nature* **2002**, *418*, 741.
(23) Magoshi, J.; Magoshi, Y.; Nakamura, S. In *Silk Polymers*; Kaplan, D., Adams, W. W., Farmer, B., Viney, C., Eds.; American Chemical Society: Washington, DC, 1994; Vol. 544, Chapter 25, p 292.
(24) Okuyama, K.; Somashekar, R.; Noguchi, K.; Ichimura, S. *Biopolymers* **2001**, *59*, 310–319.
(25) Asakura, T.; Ashida, J.; Yamane, T.; Kameda, T.; Nakazawa, Y.; Ohgo, K.; Komatsu, K. *J. Mol. Biol.* **2001**, *306*, 291–305.
(26) Asakura, T.; Yamane, T.; Nakazawa, Y.; Kameda, T.; Ando, K. *Biopolymers* **2001**, *58*, 521–525.
(27) Konishi, T.; Kurokawa, M. *Sen'I Gakkaishi* **1968**, *24*, 550–554.
(28) Lotz, B.; Keith, H. D. *J. Mol. Biol.* **1971**, *61*, 201–215.
(29) Lu, Q.; Hu, X.; Wang, X.; Kurge, J. A.; Lu, S.; Cebe, P.; Kaplan, D. L. *Acta Biomater.* **2010**, *6*, 1380–1387.
(30) Drummy, L. F.; Phillips, D. M.; Stone, M. O.; Farmer, B. L.; Naik, R. R. *Biomacromolecules* **2005**, *6*, 3328–3333.
(31) Yamane, T.; Umemura, K.; Nakazawa, Y.; Asakura, T. *Macromolecules* **2003**, *36*, 6766–6772.
(32) Wang, Y.; Kim, H. J.; Vunjak-Novakovic, G.; Kaplan, D. L. *Biomaterials* **2006**, *27*, 6064–6082.
(33) Vepari, C.; Kaplan, D. L. *Prog. Polym. Sci.* **2007**, *32*, 991–1007.
(34) Magoshi, J.; Magoshi, Y.; Nakamura, S. *J. Appl. Polym. Sci.: Appl. Polym. Symp.* **1985**, *41*, 187–204.
(35) Takahashi, Y.; Gehoh, M.; Yuzuriha, K. *Int. J. Biol. Macromol.* **1999**, *24*, 127–138.
(36) Martel, A.; Burghammer, M.; Davies, R. J.; Riekel, C. *Biomacromolecules* **2007**, *8*, 3548–3556.
(37) Du, N.; Liu, X. Y.; Narayanan, J.; Li, L.; Lim, M. L.; Li, D. *Biophys. J.* **2006**, *91*, 4528–4535.
(38) Jin, H. J.; Kaplan, D. L. *Nature* **2003**, *424*, 1057–1061.
(39) Putthanarat, S.; Stribeck, N.; Fossey, S. A.; Eby, R. K.; Adams, W. W. *Polymer* **2000**, *41*, 7735–7747.
(40) van Beek, J. D.; Hess, S.; Vollrath, F.; Meier, B. H. *Proc. Natl. Acad. Sci. U. S. A.* **2002**, *99*, 10266–10271.
(41) Oroudjev, E.; Soares, J.; Arcidiacono, S.; Thompson, J. B.; Fossey, S. A.; Hansma, H. G. *Proc. Natl. Acad. Sci. U. S. A.* **2002**, *99*, 6460–6465.
(42) Yoshioka, T.; Dersch, R.; Tsuji, M.; Schaper, A. K. *Polymer* **2010**, *51*, 2383–2389.
(43) Termonia, Y. *Macromolecules* **1994**, *27*, 7378–7381.
(44) Ene, R.; Papadopoulos, P.; Kremer, F. *Soft Matter* **2009**, *5*, 4568–4574.
(45) Kongkhlang, T.; Tashiro, K.; Kotaki, M.; Chirachanchai, S. *J. Am. Chem. Soc.* **2008**, *130*, 15460–15466.
(46) Sirichaisit, J.; Brookes, V. L.; Young, R. J.; Vollrath, F. *Biomacromolecules* **2003**, *4*, 387–394.
(47) Scheibel, T. *Microb. Cell Fact.* **2004**, *3*, 14.
(48) Hakimi, O.; Knight, D. P.; Vollrath, F.; Vadgama, P. *Composites, Part B* **2007**, *38*, 324–337.